Available online at www.sciencedirect.com

ScienceDirect

Ceramics International 40 (2014) 4623–4630

CERAMICS INTERNATIONAL

www.elsevier.com/locate/ceramint

Comparison of $(BiO)_2CO_3$ to $CdCO_3$ as anode materials for lithium-ion batteries

Lianyi Shao, Songying Wang, Kaiqiang Wu, Miao Shui, Rui Ma, Dongjie Wang, Nengbing Long, Yuanlong Ren, Jie Shu*

Faculty of Materials Science and Chemical Engineering, Ningbo University, Ningbo 315211, Zhejiang Province, People's Republic of China

Received 22 August 2013; received in revised form 31 August 2013; accepted 31 August 2013
Available online 6 September 2013

Abstract

Comparison of $(BiO)_2CO_3$ to $CdCO_3$ as anode materials is investigated in this paper. Electrochemical results show that both $(BiO)_2CO_3$ and $CdCO_3$ are electrochemically active materials with high initial capacities of 1080.1 and 1251.1 mAh g^{-1}, respectively. *Ex-situ* X-ray diffraction (XRD) results show that the electrochemical reaction mechanisms of $CdCO_3$ with Li can be associated with the preliminary formation of Cd and Li_2CO_3 upon the initial lithiation, and then the final formation of LiCd alloy upon further lithiation. In contrast, the electrochemical reaction of $(BiO)_2CO_3$ with Li not only results in the formation of Bi and Li_2CO_3, but also induces the formation of Li_2O. Besides, upon further lithiation, the alloying reaction of Bi with Li is a multi-step process to form LiBi, Li_xBi, and finally Li_3Bi as confirmed by electrochemical behaviors and *in-situ* XRD technique. Compared with $CdCO_3$, $(BiO)_2CO_3$ can exhibit better electrochemical properties with a reversible capacity of 155.1 mAh g^{-1} and a capacity retention of 28.3% after 15 cycles. By introducing carbon black as conductive additive and volume change buffer, the reversible capacity of ball-milled $(BiO)_2CO_3$/C composite can be improved to the value of 297.6 mAh g^{-1} with a capacity retention of 47.8% after 15 cycles.

Keywords: A. Milling; B. X-ray methods; C. Electrical properties; E. Batteries

1. Introduction

Since their first commercialization in the early 1990s, lithium-ion batteries have permeated from the portable electronics field to electric vehicles industry. One critical component of a lithium-ion battery is the anode material, which determines much of the energy and power densities of the rechargeable lithium-ion battery. Nowadays, graphite-based materials dominate the main market of commercial anode materials. However, the lithiation potential of commercial graphite-based anode material is too close to the deposition potential of metal Li, which may result in a high risk of dangerous lithium dendrite formation and generate critical safety concerns. Consequently, further improvements in terms of power density, safety, lifetime and cost require new materials with higher storage capacity, long cycling life and desired potentials to satisfy the commercial requirements [1].

Through the search for alternatives to commercial carbonaceous materials, large amounts of inorganic compounds have been reported recently, such as transition metal oxides (M_xO_y, where M is Co, Ni, Cu, Fe) [2–5], transition metal sulfides (M_xS_y, where M is Co, Ni, Cu, Fe) [6,7], and transition metal nitrides (M_xN_y, where M is Co, Ni, Cu, Fe) [8,9]. It is proved that the electrochemical reaction of these transition metal compounds with Li is a conversion reaction [10,11], whose mechanism is that the active materials completely reduce to metals together with the formation of lithium oxides, sulfides or nitrides during the lithiation process and then the formed products will recover to the original phase upon de-lithiation. These inorganic compounds based on conversion reaction are promising anode materials for lithium-ion batteries due to their high theoretical capacity, high safety and low cost [12,13].

Recently, similar reversible electrochemical response has been found in metal carbonates [14–18]. Our group also

*Corresponding author. Tel.: +86 574 87600787; fax: +86 574 87609987.
E-mail addresses: sergio_shu@hotmail.com, shujie@nbu.edu.cn (J. Shu).

0272-8842/$ - see front matter © 2013 Elsevier Ltd and Techna Group S.r.l. All rights reserved.
http://dx.doi.org/10.1016/j.ceramint.2013.08.140

focused on the development of various metal carbonates, such as $MnCO_3$ [19] and $CoCO_3$ [20], as lithium storage materials. These studies revealed that metal carbonates can be used directly as energy storage electrodes in lithium-ion batteries. Compared with oxides or fluorides, similar important values of reversible capacity and high capacity retention can be observed for metal carbonates.

In the present work, we investigated and compared the electrochemical properties of $(BiO)_2CO_3$ and $CdCO_3$ as anode materials for lithium-ion batteries by cyclic voltammetry and galvanostatic charge–discharge techniques. A comparison of $(BiO)_2CO_3$ to $CdCO_3$ is carried out based on lithium storage behaviors, which suggests that $(BiO)_2CO_3$ is a probable lithium storage material as an anode material for lithium-ion batteries. In addition, in order to better understand the lithium storage mechanism in $(BiO)_2CO_3$, we have utilized *ex-situ* and *in-situ* XRD techniques to make a careful study of the structural evolutions of $(BiO)_2CO_3$ during repeated electrochemical charge–discharge cycles.

2. Experimental

Commercial $(BiO)_2CO_3$ (Aladdin Chemistry Co. Ltd) and $CdCO_3$ (Aladdin Chemistry Co. Ltd) were purchased and used after ball-milling for 10 h at a milling speed of 400 r min^{-1} in the experiment. $(BiO)_2CO_3$/C composite was prepared by high energy ball milling of $(BiO)_2CO_3$ and carbon black with a weight ratio of 3:1 in a zirconia container for 10 h at a milling speed of 400 r min^{-1}.

X-ray diffraction patterns of powder samples were investigated by a Bruker AXS D8 Focus diffractometer with Cu Kα radiation ($\lambda = 0.15406$ nm). Scanning electron microscopy (SEM) images were obtained with a JEOL S3400 microscope. Thermogravimetric (TG) and differential thermal analysis (DTA) curves were obtained by a Seiko TG/DTA 6300 instrument over a temperature range between 20 to 800 °C with a heating rate of 5 °C min^{-1} under argon atmosphere.

For electrochemical tests, the simulated batteries were constructed using the metal carbonate as working electrode and lithium metal discs (Jiangxi Ganfeng Lithium Co. Ltd) as counter and reference electrodes. The working electrode was fabricated by blending a mixture of active materials, conductive carbon black, and polyvinylidene fluoride binder in a weight ratio of 6:3:1 dissolved in N-methyl-pyrrolidone. Shortly afterwards, the slurry was cast onto a Cu foil and dried at 120 °C for 12 h in a vacuum oven and then cut into discs with a diameter of 15 mm. The electrolyte was 1 mol L^{-1} $LiPF_6$ (Zhangjiagang Guotai Huarong New Chemical Materials Co. Ltd) in a nonaqueous solution of ethylene carbonate and dimethyl carbonate with a volume ratio of 1:1. The simulated batteries were assembled in a glove box with high-purity argon atmosphere.

Galvanostatic charge–discharge experiments for simulated batteries were tested at a constant current density of 50 mA g^{-1} in 0.0–3.0 V by a multichannel Land2001A battery test system (Wuhan Jinnuo, China) at room temperature. In addition, cyclic voltammogram (CV) tests were carried out by a CHI 1000B electrochemical workstation (Shanghai Chenhua, China) with a scanning rate of 0.1 mV s^{-1} at room temperature. Electrochemical impedance spectra were collected by a CHI 660D electrochemical workstation (Shanghai Chenhua, China) with the frequency range between 100,000 and 0.01 Hz at room temperature.

In order to gain insight into the electrochemical working mechanisms of metal carbonates ($(BiO)_2CO_3$ and $CdCO_3$) with lithium, *in-situ* and *ex-situ* XRD measurements were performed on the lithiated and delithiated samples during the initial charge–discharge cycle. The lithiated and delitiated samples for *ex-situ* XRD were prepared by taking out the cycled electrodes from disassembled batteries and dried under vacuum condition. The structure and equipment of the *in-situ* XRD battery were described in our previous paper [21].

3. Results and discussion

The phase structures of $(BiO)_2CO_3$ and $CdCO_3$ are displayed in Fig. 1. Based on the JCPDS Card no. 84-1752, the main diffraction peaks at 12.7°, 23.9°, 30.3° and 32.8° can be attributed to the (040), (121), (161) and (002) reflections of the orthorhombic structure of $(BiO)_2CO_3$ as shown in Fig. 1a. For the main diffraction peaks appeared at 23.6°, 30.4°, 36.6°, 43.9° and 50.1° in Fig. 1b, they can be indexed to the structural characteristics of the rhombohedral $CdCO_3$ (JCPDS

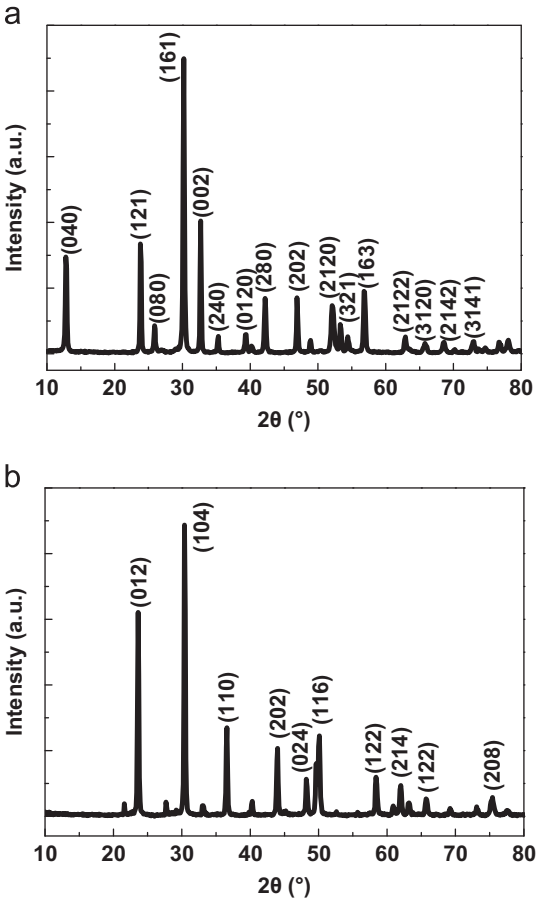

Fig. 1. XRD patterns of (a) $(BiO)_2CO_3$ and (b) $CdCO_3$.

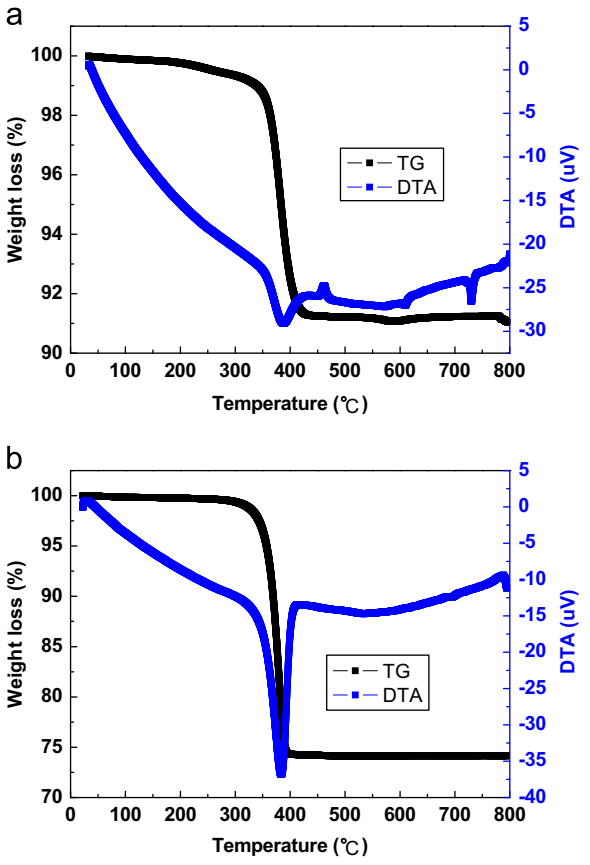

Fig. 2. TG–DTA curves of (a) $(BiO)_2CO_3$ and (b) $CdCO_3$.

Card no. 42-1342). Therefore, it is obvious that both samples are high purity materials.

The safety issue is the main obstacle for lithium storage materials to be used as commercial electrodes for lithium-ion batteries. Here, the thermal properties (TG–DTA curves) of $(BiO)_2CO_3$ and $CdCO_3$ are shown in Fig. 2a and b. For $(BiO)_2CO_3$, the observed weight loss of 8.67% at around 400.0 °C agrees perfectly with the theoretical value of 8.63% due to the removal of CO_2, revealing the decomposition of $(BiO)_2CO_3$ to form Bi_2O_3 and CO_2 in this process. In addition, there are two main endothermic peaks at 388.9 and 730.8 °C as well as one exothermic peak at 463.2 °C in the DTA curve, corresponding to three evident phase transition processes of Bi_2O_3 [22]. In turn, the thermal decomposition of $CdCO_3$ also takes place by a single step in the TG curve, leading to the formation of CdO and CO_2 above 396.3 °C [23,24]. The theoretical weight change from $CdCO_3$ to CdO agrees well with the step in the experimental TG curve. Therefore, both $(BiO)_2CO_3$ and $CdCO_3$ samples exhibit high thermal stabilities below 380 °C, which can satisfy the requirements for applications in lithium-ion batteries.

Fig. 3a and b exhibits the SEM images of $(BiO)_2CO_3$ and $CdCO_3$. Fig. 3a shows the surface morphology of $(BiO)_2CO_3$ sample, which is composed of ample amount of irregular nanosheets with a length of around 200 nm and a thickness of around 25 nm. For comparison, $CdCO_3$ samples display the

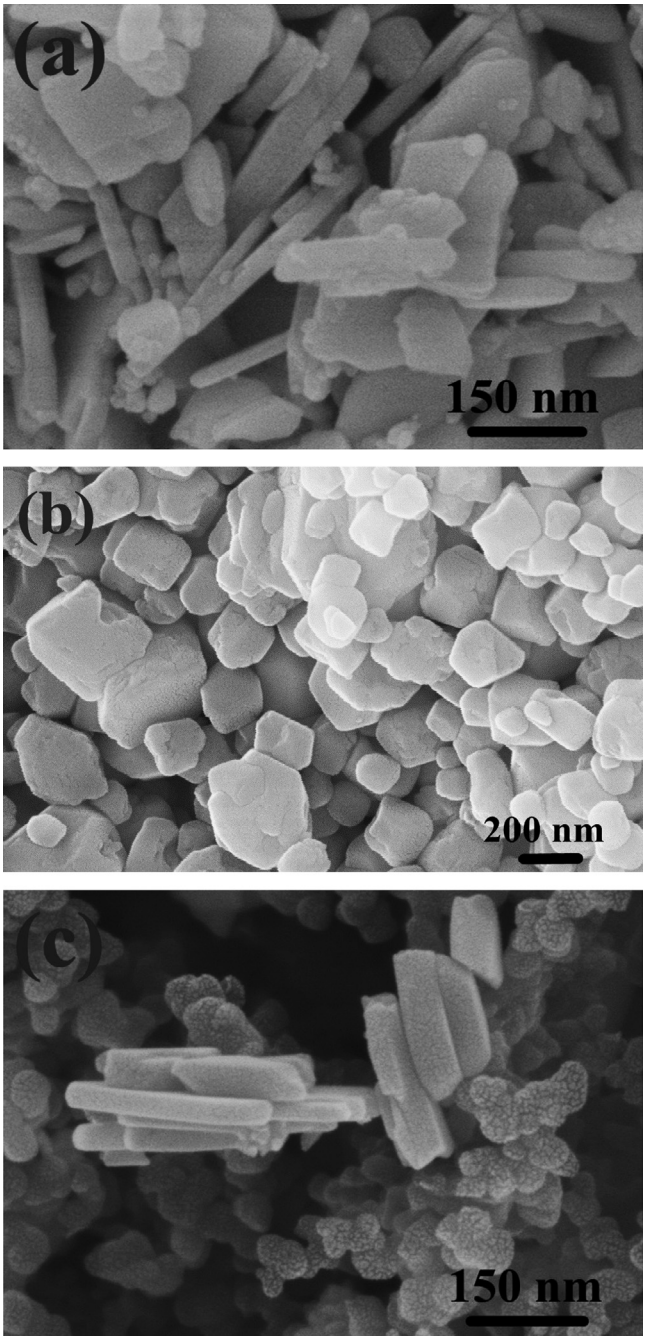

Fig. 3. SEM images of (a) $(BiO)_2CO_3$, (b) $CdCO_3$ and (c) $(BiO)_2CO_3$/C composite after ball-milling.

morphology of ball-shaped particles with the diameter ranging from 200 to 300 nm as shown in Fig. 3b.

The CV curves of the initial three cycles for $(BiO)_2CO_3$ and $CdCO_3$ over a potential range of 0.0–3.0 V are shown in Fig. 4. In the first discharge process for $(BiO)_2CO_3$ as shown in Fig. 4a, three cathodic peaks are observed at 1.59 V (strong), 1.34 V (moderate) and 0.57 V (strong). The corresponding three anodic peaks can be found at 2.45 V (weak), 1.59 V (weak) and 0.98 V (strong) during the first charge process. With further cycling, the intensities of these peaks weaken compared with those of the first cycle. The strong

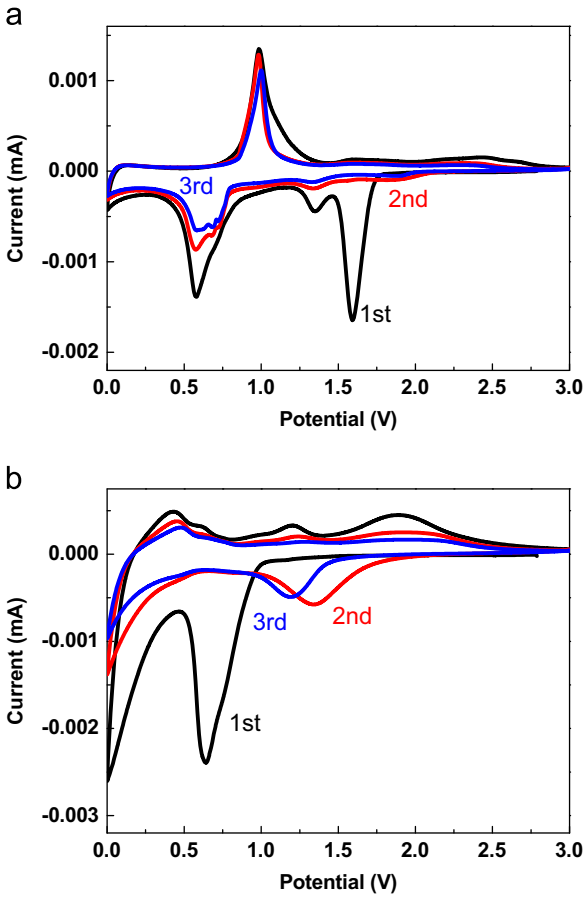

Fig. 4. Cyclic voltammogram curves of (a) $(BiO)_2CO_3$ and (b) $CdCO_3$.

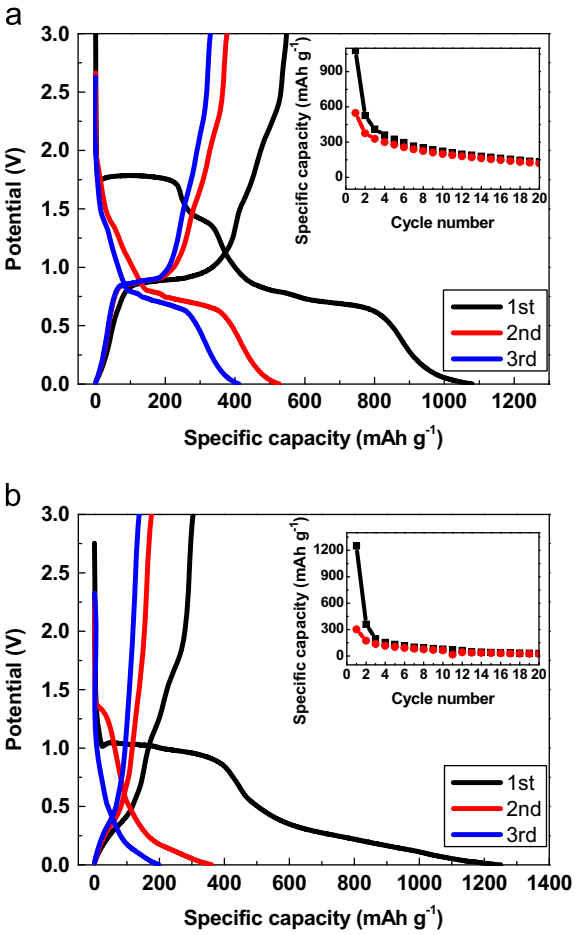

Fig. 5. Charge–discharge curves and corresponding cyclic performances of (a) $(BiO)_2CO_3$ and (b) $CdCO_3$ at a current density of 50 mA g^{-1} between 0.0 and 3.0 V.

reversible anodic/cathodic couple at 0.98/0.57 V may be attributed to the alloying/de-alloying reaction between Bi and Li. The existence of another two asymmetry couples of cathodic/anodic peaks reveals that the electrochemical conversion reaction of $(BiO)_2CO_3$ with Li should be composed of at least two other irreversible steps, which will be discussed in detail in the following section.

In the case of $CdCO_3$ (Fig.4b), two reduction peaks and four oxidation peaks are detected in the initial scanning. The reduction peak at 0.64 V can be attributed to the reaction between $CdCO_3$ and Li as well as the formation of solid electrolyte interphase (SEI) film [25]. The reduction peak at around 0.00 V and the first two oxidation peaks at 0.42 and 0.62 V may be ascribed to the lithium insertion and extraction from active metal material, Cd. In the following cycles, the redox couple at 1.34/1.93 V is probably attributed to the decomposition/formation of $CdCO_3$. Upon repeated cycles, the reduction peak shifts to higher potentials owing to the decrease of polarization, the decomposition of the electrolyte and the formation of SEI film. These results are in accordance with those of charge–discharge tests.

The charge–discharge curves and corresponding cyclic performances of $(BiO)_2CO_3$ and $CdCO_3$ are given and compared in Fig. 5a and b. The lithiation/delithiation plateaus in the charge–discharge profiles (Fig. 5a and b) are consistent with the CV curves as shown in Fig. 4a and b. The $(BiO)_2CO_3$ exhibits a discharge specific capacity of 1080.1 mAh g^{-1} and a charge specific capacity of 547.9 mAh g^{-1} in the initial cycle, corresponding to a coulombic efficiency of 50.7%. The irreversible capacity can be ascribed to the formation of SEI film and the electrochemical inactivity of partial inserted Li after the initial cycle. After 20 cycles, $(BiO)_2CO_3$ just remains a charge specific capacity of 119.9 mAh g^{-1} with a capacity retention of 21.9%. The poor cycling behavior can be associated with the large volume change occurring during charge–discharge cycles and the pulverization of active material during Li insertion [26]. Similar to the electrochemical property of $(BiO)_2CO_3$, $CdCO_3$ delivers a discharge specific capacity of 1251.1 mAh g^{-1} and a charge specific capacity of 303.5 mAh g^{-1} in the initial cycle, corresponding to an initial coulombic efficiency of 24.3%. And the charge capacity of $CdCO_3$ is only 23.9 mAh g^{-1} with a capacity retention of 7.87% after 20 cycles. Therefore, it is obvious that $(BiO)_2CO_3$ is more suitable for lithium-ion batteries to be used as anode material compared with $CdCO_3$.

To identify the lithium storage mechanisms in $(BiO)_2CO_3$ and $CdCO_3$, *ex-situ* XRD measurements were carried out for structural evolution investigation. We assembled eleven simulated batteries in the *ex-situ* XRD experiment. Among these

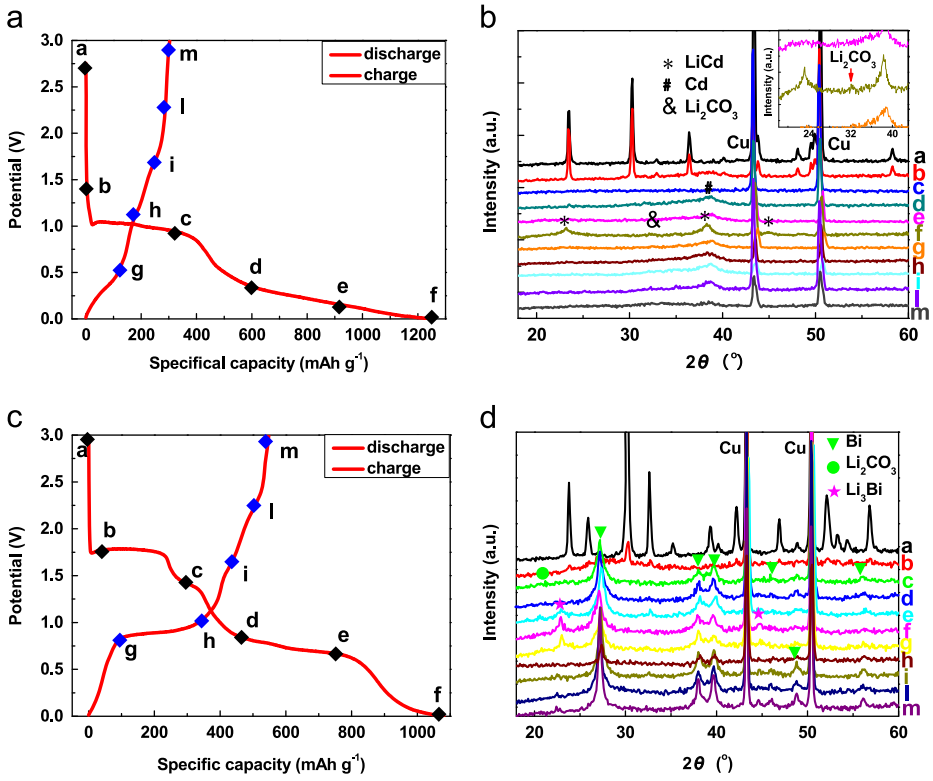

Fig. 6. Lithiated and delithiated samples obtained for *ex-situ* XRD analysis and corresponding *ex-situ* XRD patterns during the initial charge–discharge process. (a and b) $CdCO_3$; (c and d) $(BiO)_2CO_3$.

eleven batteries, we prepared six lithiated samples with the names of (a), (b), (c), (d), (e) and (f) as shown in Fig. 6a and c. In the reverse charge process, five delithiated samples are named as (g), (h), (i), (l) and (m).

As the *ex-situ* XRD patterns shown in Fig. 6b, the featured diffraction peaks of $CdCO_3$ gradually disappear along lithiation. At the same time, the appearance of diffraction peak at 38.4° corresponds to the (101) plane of metal Cd in JCPDS Card no. 85-1328, indicating the phase transition from $CdCO_3$ to Cd. Upon further lithiation, the phase transition from Cd to LiCd can be observed according to the appearance of the diffraction peaks at 23.0°, 38.0° and 44.9°, which bragg positions can be attributed to the (111), (220) and (311) planes of LiCd alloy in JCPDS Card no. 03-0916. For the final lithiated sample, the weak peak located at 32.1° can be identified to the (002) plane of Li_2CO_3 (JCPDS Card no. 83-1454) in the XRD patterns. During further delithiation, the diffraction peaks of Li_2CO_3 and LiCd disappear in the initial charge process, and then the featured peak of Cd also gradually disappears. Upon recharge to 3.0 V, no diffraction peaks of the delithiated sample can be observed as shown in Fig. 6b, indicating an amorphous structure of final product. As reported, this phenomenon also exists in the electrochemical cycles of metal hydroxides and cobalt chlorides [27,28]. Furthermore, the reversible redox peaks in Fig. 4b suggest that the probable re-formation of the pristine sample. Based on the above *ex-situ* XRD results and reversible CV curves, the involved electrochemical reactions during the initial charge–discharge cycle can be described as follows:

$$CdCO_3 + 2Li^+ + 2e^- \leftrightarrow Cd + Li_2CO_3$$

$$Cd + Li^+ + e^- \leftrightarrow LiCd$$

For $(BiO)_2CO_3$, the XRD pattern of sample discharged to a definite capacity shows that all the diffraction peaks of $(BiO)_2CO_3$ disappear during the initial discharge process, indicating the complete structural destruction of the pristine sample. Simultaneously, an interesting observation is the appearance of the characteristic diffraction peaks of new phases, which are indexed to metal Bi (JCPDS Card no. 85-1329) at 27.2° (012), 38.0° (104), 39.6° (110), 45.8° (006), 48.7° (202), 56.0° (024) and Li_2CO_3 (JCPDS Card no. 83-1454) at 21.4° (200). With a discharge process to 0.0 V, some of Bi phases transform into Li_3Bi (JCPDS card no. 27-0427) phase as shown in Fig. 6d. During the reverse charge process, the Li_3Bi phase disappears and the diffraction peaks of Bi phase become stronger. Finally, only the diffraction peaks of Bi phase can be observed when the sample is fully charged to 3.0 V.

The results of *ex-situ* XRD experiments indicate that the initial discharge process leads to the formation of Li_xM (M=Cd or Bi) and Li_2CO_3 with a collapse of the pristine structure of active material ($(BiO)_2CO_3$ or $CdCO_3$). Furthermore, the original structure of active material cannot be totally recovered after the initial charge process. This lithium storage mechanism could explain the existence of remarkable potential

and capacity differences between the initial and subsequent discharge curves.

According to the CV behaviors of $(BiO)_2CO_3$ in Fig. 4a, three reversible reduction peaks appeared at 0.58, 0.68 and 0.72 V. It indicates that the electrochemical reaction between Li and Bi is a complex process. In order to further clarify the alloying reaction between Li and Bi, we made a thorough investigation about the structural evolutions of $(BiO)_2CO_3$ by using an *in-situ* XRD technique. The diffraction peaks at 38.5°, 41.2° and 43.9° are attributed to the beryllium oxide layer on X-ray window according to the JCPDS Card no. 78-1553 and previous reports [29,30] as shown in Fig. 7a. The characteristic diffraction peaks of $(BiO)_2CO_3$ gradually disappear along lithiation. Simultaneously, new diffraction peaks at 33.6°, 38.0° and 22.9° appear in the discharge process, corresponding to the formation of Li_2O (JCPDS Card no. 77-2144), Bi (JCPDS Card no. 85-1329) and Li_3Bi (JCPDS Card no. 27-0427), respectively. Besides, three unknown diffraction peaks at 24.6°, 25.5° and 35.0° appeared in the middle of discharge process (Fig. 7b) may be attributed to the appearance of unidentified Li_xBi intermediate phase. These phase transitions can be consistent with the three reversible reduction peaks that appeared at 0.58, 0.68 and 0.72 V. In the reverse charge process, the intensity change of the diffraction peaks at 27.1°, 37.9° and 39.6° can be attributed to the transformation from Li_3Bi to Bi. At the fully charged state (3.0 V), only the Bi phase can be detected in Fig. 7a. According to the above results and previous reports on bismuth compounds as lithium storage materials [26,31], it can be deduced that $(BiO)_2CO_3$ reacts with Li according to the following conversion reactions:

$$(BiO)_2CO_3 + 6Li^+ + 6e^- \rightarrow 2Bi + Li_2CO_3 + 2Li_2O$$

$$Bi + 3Li^+ + 3e^- \leftrightarrow Li_3Bi$$

Although no diffraction peaks of $(BiO)_2CO_3$, Bi_2O_3 and $Bi_2(CO_3)_3$ can be detected, two weak redox couples at 1.34/1.59 and 1.87/2.31 V can still be observed in CV curves as shown in Fig. 4a. Therefore, the oxidation of Bi, Li_2CO_3 and Li_2O may result in the trace formation of Bi_2O_3 and $Bi_2(CO_3)_3$.

In addition, based on the proposed reactions, it should be noted that the initial discharge specific capacity (1080.1 mAh g^{-1}) of $(BiO)_2CO_3$ is much higher than the theoretical capacity (630.1 mAh g^{-1}), which may be attributed to the organic solvent reduction reaction and the probable reduction of CO_3^{2-} to low valence carbon [17,20,32]. However, the cycling properties of $(BiO)_2CO_3$ is poor with a capacity retention of 21.9% after 20 cycles. In order to improve the cycling performance of $(BiO)_2CO_3$, $(BiO)_2CO_3$ and carbon black are mixed by using high energy ball milling with a weight ratio of 3:1 in a zirconia container for 10 h to obtain well-dispersed particles and carbon buffers. As shown in Fig. 3a and c, the average particle size of ball-milled $(BiO)_2CO_3$/C composite is similar to the average particle size of pure $(BiO)_2CO_3$ after high-energy ball-milling. Moreover, the active materials are well-dispersed and surrounded by conductive carbon black particles, which will improve the electronic conductivity of $(BiO)_2CO_3$ and hinder the structural breakdown of active materials.

Fig. 8a compares the charge–discharge curves of the pristine $(BiO)_2CO_3$ and ball-milled $(BiO)_2CO_3$/C composite. It is obvious that the ball-milled $(BiO)_2CO_3$/C composite delivers a discharge capacity of 1150.8 mAh g^{-1} and a charge capacity of 620.9 mAh g^{-1} in the initial cycle, corresponding to a coulombic efficiency of 54.0%. The capacity retention of the ball-milled $(BiO)_2CO_3$/C composite is enhanced to 47.9% compared with that of $(BiO)_2CO_3$ as shown in Fig. 8b. After 15 cycles, the reversible charge capacity of ball-milled $(BiO)_2CO_3$/C composite is 297.6 mAh g^{-1}, which is much higher than that (155.1 mAh g^{-1}) of the pristine $(BiO)_2CO_3$. The enhanced electrochemical properties of $(BiO)_2CO_3$/C can be attributed to the buffering effect and high electronic conductivity of carbon black and the well-dispersed active particles which can improve the charge transfer process between material and electrolyte as the electrochemical impedance spectra shown in Fig. 9.

Table 1 describes the equivalent circuit parameters of $(BiO)_2CO_3$ and ball-milled $(BiO)_2CO_3$/C composite before and after cycles. These equivalent circuit parameters are calculated from the spectra in Fig. 9 and fitted by ZView software. Here, R_s, R_f and R_{ct} are solution resistance, SEI film resistance and charge transfer resistance, respectively. It is

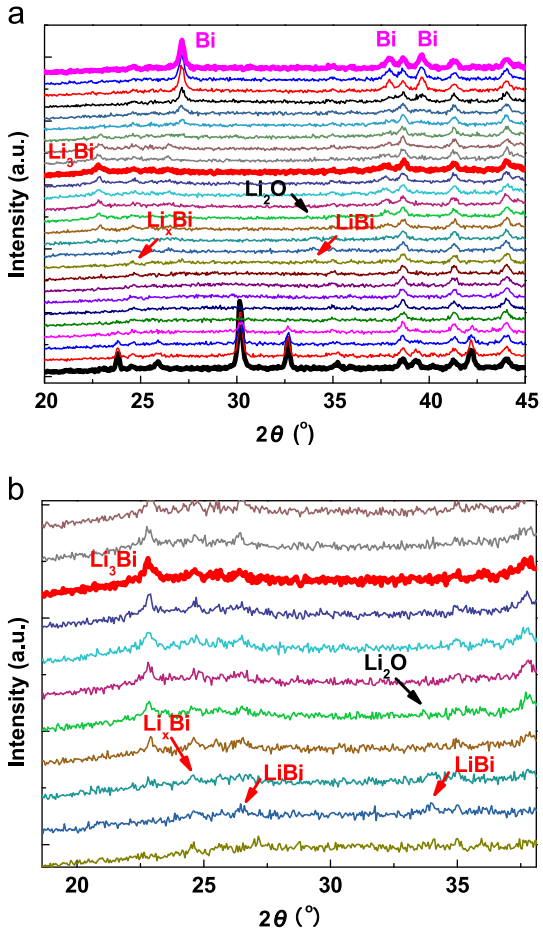

Fig. 7. *In-situ* XRD patterns of $(BiO)_2CO_3$ cycled between 0.0 and 3.0 V at a current density of 50 mA g^{-1}. (a) Full-view patterns; and (b) selected patterns.

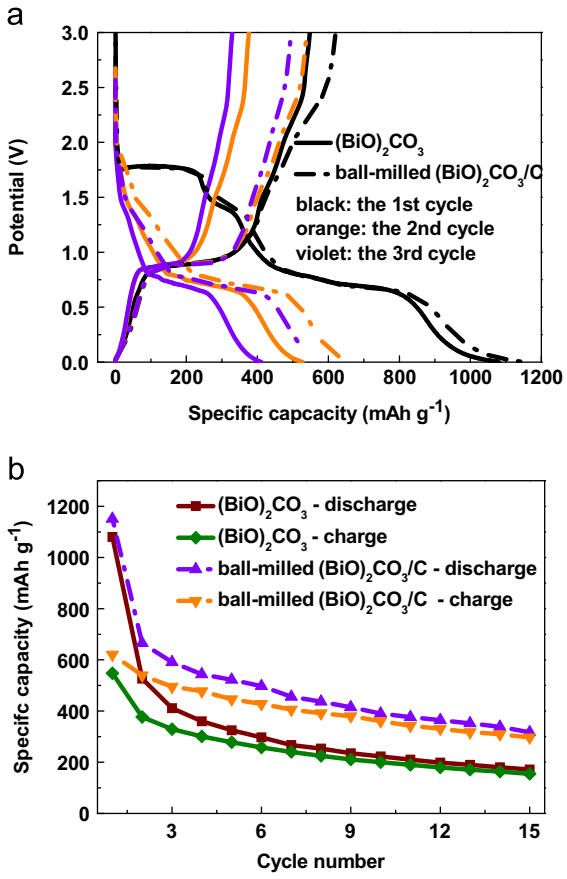

Fig. 8. (a) Charge–discharge curves and (b) corresponding cyclic performances of $(BiO)_2CO_3$ and ball-milled $(BiO)_2CO_3$/C composite at a current density of 50 mA g^{-1} between 0.0 and 3.0 V.

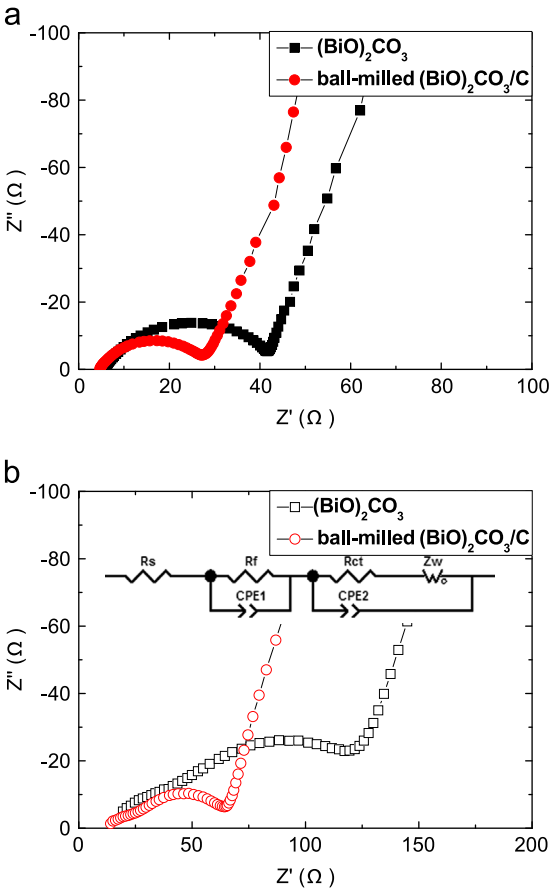

Fig. 9. Electrochemical impedance spectra of $(BiO)_2CO_3$, and ball-milled $(BiO)_2CO_3$/C composite before (a) and after cycles (b).

clear that the introduction of conductive carbon black decreases the solution resistance from 5.985 to 4.672 Ω and charge transfer resistance from 38.265 to 24.603 Ω. After repeated charge–discharge cycles, both solution resistance and charge transfer resistance show an obvious increase. Besides, the resistance for the formation of SEI film also appears due to the electrolyte irreversible decomposition. Based on the data of R_f and R_{ct}, it is clear that the deterioration of $(BiO)_2CO_3$ electrode is more serious than that of ball-milled $(BiO)_2CO_3$/C composite. Therefore, the capacity retention of 47.9% for ball-milled $(BiO)_2CO_3$/C composite is also much higher the value of 28.3% for $(BiO)_2CO_3$. It suggests that the introduction of conductive carbon black buffers improves the reversible lithium storage capacity and cycling calendar life of $(BiO)_2CO_3$.

Table 1
Equivalent circuit parameters of $(BiO)_2CO_3$ and ball-milled $(BiO)_2CO_3$/C composite before and after cycles.

Sample	R_s (Ω)	R_f (Ω)	R_{ct} (Ω)
$(BiO)_2CO_3$-Before cycles	5.985	–	38.265
$(BiO)_2CO_3$/C-Before cycles	4.672	–	24.603
$(BiO)_2CO_3$-After cycles	8.583	40.044	108.923
$(BiO)_2CO_3$/C-After cycles	6.826	24.674	40.527

4. Conclusions

As an anode material for lithium-ion batteries, it can be found that $(BiO)_2CO_3$ shows an initial discharge specific capacity of 1080.1 mAh g^{-1} and a charge specific capacity of 547.9 mAh g^{-1} at a current density of 50 mA g^{-1} between 0.0 and 3.0 V, and remains a capacity retention of 21.9% after 20 cycles. Although $CdCO_3$ can deliver a higher discharge specific capacity (1251.1 mAh/g) compared with $(BiO)_2CO_3$, its cycling performance is much poorer with a reversible capacity of 23.9 mAh g^{-1} after 20 cycles owing to structure instability and poor electronic conductivity. *Ex-situ* and *in-situ* XRD results show the structural evolutions of $(BiO)_2CO_3$ and $CdCO_3$ during the initial charge–discharge cycle. For $CdCO_3$, *ex-situ* XRD results show that the initial discharge process leads to the pulverization of active particles and the collapse of structure due to the formation of LiCd and Li_2CO_3, and then not only the pristine structure of $CdCO_3$ cannot be restored reversibly in the charge process but also metal Cd cannot be observed at the end of charge, indicating the low-degree reversibility of $CdCO_3$ electrode. Combining the *ex-situ* and *in-situ* XRD results, it is obvious that the initial electrochemical reaction of $(BiO)_2CO_3$ with Li is related to the formation of Bi, Li_2O and Li_2CO_3 and then the alloying reaction of Bi with

Li takes place in low potential region. Upon delithiation, the re-appearance of metal Bi can be observed, indicating the high-degree reversibility of $(BiO)_2CO_3$ electrode. To improve the electrochemical properties of $(BiO)_2CO_3$, carbon black is introduced by using as conductive additive and volume change buffer. As a result, $(BiO)_2CO_3$/C composite can deliver a higher reversible specific capacity (297.6 mAh g^{-1}) than that (155.1 mAh g^{-1}) of pure $(BiO)_2CO_3$ after 15 cycles, indicating that conductive carbon buffers are beneficial to obtain high lithium storage capacity and excellent cycling life.

Acknowledgements

This work is sponsored by the National 863 Program (2013AA050901) and National Natural Science Foundation of China (No. 51104092). The work is also supported by Graduate Student Research and Innovation Program (G13034) and K.C. Wong Magna Fund in Ningbo University.

References

[1] H.L Chen, G. Hautier, A. Jain, C. Moore, B. Kang, R. Doe, L.J. Wu, Y.M. Zhu, Y.Z. Tang, G. Ceder, Carbonophosphates: a new family of cathode materials for Li-ion batteries identified computationally, Chemistry of Materials 24 (2012) 2009–2016.

[2] X.Y. Yao, X. Xin, Y.M. Zhang, J. Wang, Z.P. Liu, X.X. Xu, Co_3O_4 nanowires as high capacity anode materials for lithium ion batteries, Journal of Alloys and Compounds 521 (2012) 95–100.

[3] A.K. Rai, L.T. Anh, C.J. Park, J. Kim, Electrochemical study of NiO nanoparticles electrode for application in rechargeable lithium-ion batteries, Ceramics International 39 (2013) 6611–6618.

[4] S.D. Seo, D.H. Lee, J.C. Kim, G.H. Lee, D.W. Kim, Room-temperature synthesis of CuO/graphene nanocomposite electrodes for high lithium storage capacity, Ceramics International 39 (2013) 1749–1755.

[5] S.L. Jin, H.G. Deng, D.H. Long, X.J. Liu, L. Zhan, X.Y. Liang, W.M. Qiao, L.C. Ling, Facile synthesis of hierarchically structured Fe_3O_4/carbon micro-flowers and their application to lithium-ion battery anodes, Journal of Power Sources 196 (2011) 3887–3893.

[6] J.M. Yan, H.Z. Huang, J. Zhang, Z.J. Liu, Y. Yang, A study of novel anode material CoS_2 for lithium ion battery, Journal of Power Sources 146 (2005) 264–269.

[7] C.C. Dong, X.D. Zheng, B. Huang, M. Lu, Enhanced electrochemical performance of FeS coated by Ag as anode for lithium-ion batteries, Applied Surface Science 265 (2013) 114–119.

[8] B. Das, M.V. Reddy, P. Malar, T. Osipowicz, G.V.S. Rao, B.V.R. Chowdari, Nanoflake CoN as a high capacity anode for Li-ion batteries, Solid State Ionics 180 (2009) 1061–1068.

[9] Q. Sun, Z.W. Fu, Vanadium nitride as a novel thin film anode material for rechargeable lithium batteries, Electrochimica Acta 54 (2008) 403–409.

[10] G.X. Wang, Y. Chen, K. Konstantinov, M. Lindsay, H.K. Liu, S.X. Dou, Investigation of cobalt oxides as anode materials for Li-ion batteries, Journal of Power Sources 109 (2002) 142–147.

[11] Q. Sun, Z.W. Fu, Mn_3N_2 as a novel negative electrode material for rechargeable lithium batteries, Applied Surface Science 258 (2012) 3197–3201.

[12] Y.M. Kang, K.T. Kim, J.H. Kim, H.S. Kim, P.S. Lee, J.Y. Lee, H.K. Liu, S.X. Dou, Electrochemical properties of Co_3O_4, Ni–Co_3O_4 mixture and Ni–Co_3O_4 composite as anode materials for Li ion secondary batteries, Journal of Power Sources 133 (2004) 252–259.

[13] X.Y. Yan, X.L. Tong, J. Wang, C.W. Gong, M.G. Zhang, L.P. Liang, Hydrothermal-synthesized NiO nanowall array for lithium ion batteries, Journal of Alloys and Compounds 556 (2013) 56–61.

[14] M.J. Aragon, B. Leon, C.P. Vicente, J.L. Tirado, A new form of manganese carbonate for the negative electrode of lithium-ion batteries, Journal of Power Sources 196 (2011) 2863–2866.

[15] S. Mirhashemihaghighi, B. Leon, C.P. Vicente, J.L. Tirado, R. Stoyanova, M. Yoncheva, E. Zhecheva, R.S. Puche, E.M. Arroyo, J.R. Paz, Lithium storage mechanisms and effect of partial cobalt substitution in manganese carbonate electrodes, Inorganic Chemistry 51 (2012) 5554–5560.

[16] M.J. Aragon, B. Leon, C.P. Vicente, J.L. Tirado, On the use of transition metal oxysalts as conversion electrodes in lithium-ion batteries, Journal of Power Sources 196 (2011) 2863–2866.

[17] L.W. Su, Z. Zhou, X. Qin, Q.W. Tang, D.H. Wu, P.W. Shen, $CoCO_3$ submicrocube/grapheme composites with high lithium storage capability, Nano Energy 3 (2013) 276–282.

[18] Z.J. Ding, B. Yao, J.K. Feng, J.X. Zhang, Enhanced rate performance and cycling stability of a $CoCO_3$-polypyrrole composite for lithium ion battery anodes, Journal of Materials Chemistry A 1 (2013) 11200–11209.

[19] L.Y. Shao, J. Shu, R. Ma, M. Shui, L. Hou, K.Q. Wu, D.J. Wang, Y.L. Ren, Electrochemical characteristics and intercalation mechanism of manganese carbonate as anode material for lithium-ion batteries, International Journal of Electrochemical Science 8 (2013) 1170–1180.

[20] L.Y. Shao, R. Ma, K.Q Wu, M. Shui, M.M. Lao, D.J. Wang, N.B. Long, Y.L. Ren, J. Shu, Metal carbonates as anode materials for lithium ion batteries, Journal of Alloys and Compounds 581 (2013) 602–609.

[21] J. Shu, M. Shui, D. Xu, Y.L. Ren, D.J. Wang, Q.C. Wang, R. Ma, W.D. Zheng, S. Gao, L. Hou, J.J. Xu, J. Cui, Z.H. Zhu, Large-scale synthesis of $Li_{1.15}V_3O_8$ nanobelts and their lithium storage behavior studied by *in situ* X-ray diffraction, Journal of Materials Chemistry 22 (2012) 3035–3043.

[22] Z.H. Ai, Y. Huang, S.C. Lee, L.Z. Zhang, Monoclinic α-Bi_2O_3 photocatalyst for efficient removal of gaseous NO and HCHO under visible light irradiation, Journal of Alloys and Compounds 509 (2011) 2044–2049.

[23] B. Malecka, A. Lacz, A. Malecki, TG/DTA/MS/IR study on decomposition of cadmium malonate hydrates in inert and oxidative atmosphere, Journal of Analytical and Applied Prolysis 80 (2007) 126–133.

[24] L.M. Song, C. Chen, S.J. Zhang, Self-assembly of $CdCO_3$-dye hybrid nanotubes based on trypan blue dye, Colloids and Surfaces A: Physicochemical Engineering Aspects 374 (2011) 129–133.

[25] Y. Sharma, N. Sharma, G.V.S. Rao, B.V.R. Chowdari, Lithium-storage and cycleability of nano-$CdSnO_3$ as an anode material for lithium-ion batteries, Journal of Power Sources 192 (2009) 627–635.

[26] C.M. Park, S. Yoon, S.I. Lee, H.J. Sohn, Enhanced electrochemical properties of nanostructured bismuth-based composites for rechargeable lithium batteries, Journal of Power Sources 186 (2009) 206–210.

[27] S.B. Ni, X.H. Lv, T. Li, X.L. Yang, L.L. Zhang, The investigation of Ni (OH)2/Ni as anode for high performance Li-ion battery, Journal of Materials Chemistry A1 (2013) 1535–1544.

[28] J.L. Liu, W.J. Cui, C.X. Wang, Y.Y. Xia, Electrochemical reaction of lithium with $CoCl_2$ in nonaqueous electrolyte, Electrochemistry Communications 13 (2011) 269–271.

[29] D.D. Thorat, B.M. Tripathi, D. Sathiyamoorthy, Extraction of beryllium from Indian beryl by ammonium hydrofluoride, Hydrometallurgy 109 (2011) 18–22.

[30] J.H. Yum, T. Akyol, M. Lei, D.A. Ferrer, T.W. Hudnall, M. Downer, C.W. Bielawski, G. Bersuker, J.C. Lee, S.K. Banerjee, A study of highly crystalline novel beryllium oxide film using atomic layer deposition, Journal of Crystal Growth 334 (2011) 126–133.

[31] J.C. Peerez-Flores, A. Kuhn, F. Garcia-Alvarado, Electrochemical performances of $BiSbO_4$ as electrode material for lithium batteries, Journal of Power Sources 182 (2008) 365–369.

[32] H. Jung, C.M. Park, H.J. Sohn, Bismuth sulfide and its carbon nanocomposite for rechargeable lithium-ion batteries, Electrochimica Acta 56 (2011) 2135–2139.